WU JING (Orcid ID: 0000-0003-2513-2475)
Wang Luo (Orcid ID: 0000-0003-2217-8478)

Shrinkage of East Asia winter monsoon associated with increased ENSO events since the mid-Holocene

J. Wu[1,2], Q. Liu[1,2], Q. Y. Cui[3], D. K. Xu[1,2,4], L. Wang[1,2], C. M. Shen[5], G. Q. Chu[1,2,6], and J. Q. Liu[7,1]

[1]Key Laboratory of Cenozoic Geology and Environment, Institute of Geology and Geophysics, Chinese Academy of Sciences, Beijing 100029, China

[2]Institutions of Earth Science, Chinese Academy of Sciences, Beijing 100029, China

[3]Key Laboratory of Land Surface Pattern and Simulation, Institute of Geographical Sciences and Natural Resources Research, Chinese Academy of Sciences, Beijing 100101, China

[4]CAS Center for Excellence in Tibetan Plateau Earth Sciences, Beijing 100101, China

[5]Key Laboratory of Plateau Lake Ecology and Global Change Yunnan Normal University, Kunming 650500, China

[6]CAS Center for Excellence in Life and Paleoenvironment, Beijing 100044, China

[7]University of Chinese Academy of Sciences, Beijing 100049, China

Corresponding author: J. Wu (wujing@mail.iggcas.ac.cn); J. Q. Liu (liujq@mail.iggcas.ac.cn)

Key Points:

- A pollen record from Lake Moon in Northeast China in Holocene implies the shrinkage of the EAWM after 6 ka BP
- The teleconnection between the EAWM and El Niño events is obvious in Holocene
- Solar activity may be main driving force of the ENSO and the EAWM on centennial/millennial timescale since mid-Holocene

This article has been accepted for publication and undergone full peer review but has not been through the copyediting, typesetting, pagination and proofreading process which may lead to differences between this version and the Version of Record. Please cite this article as doi: 10.1029/2018JD030148

© 2019 American Geophysical Union. All rights reserved.

Abstract

Instrumental records indicate a close relationship between the El Niño-Southern Oscillation (ENSO) and the East Asian winter monsoon (EAWM) on interannual to decadal timescales. However, few studies have examined possible links between them on centennial/millennial time scales. In Northeast China, modern observations show that the immigration of temperate forest trees such as *Pinus* (pine) and *Quercus* (oak) into cold temperate boreal forest is sensitive to changes in winter temperature. Here we present a continuous high-resolution pollen record from Lake Moon in the central part of the Great Khingan Mountain Range, Northeast China. The record reveals increasing contents of *Pinus* and *Quercus* pollen after ~6.0 ka cal. BP, which may indicate a gradual weakening of the EAWM. It is broadly coupled with an increasing El Niño frequency since the middle Holocene, and we observe a statistically significant correlation between the percentages of *Pinus* and *Quercus* and a time series of El Niño events. On the centennial to millennial timescale, the results of wavelet analysis and band-pass filtering show that the occurrence and development of El Nino have also promoted a weaker EAWM after ~6.0 ka cal. BP, which is inversely correlated with the variation of the ca. 500-year cycle originated from changes in solar output. These results imply that the climate transition in the mid-Holocene is caused by the change of variations in solar activity and amplified by ocean circulation ENSO to influence the East Asian Monsoon system, especially the EAWM, and finally change the vegetation in Great Khingan Mountain Range.

1 Introduction

The East Asian winter monsoon (EAWM) is the most active and powerful atmospheric circulation system during the Northern Hemisphere winter. The EAWM has large environmental, societal, and economic impacts in its region of influence due to the associated severe cold surges and heavy snowfall. In addition to regional impacts, the EAWM may have a global impact through its effects on the Walker circulation. Previous studies have indicated that the EAWM and the El Niño-Southern Oscillation (ENSO) are tightly coupled [*An et al.,* 2017; *Cheung et al.,* 2012; *Li,* 1990; *Li et al.,* 2005; *Wen et al.,* 2000; *Zhou et al.,* 2007]. The ENSO is the abnormal sea surface warming or cooling phenomena affected the globe climate change, whose main center located over the tropical Pacific Ocean [*An et al.,* 2017; *Cheung et al.,* 2012]. Generally, an El Niño event weakens the EAWM leading to a positive surface temperature anomaly across most parts of China through changes in anticyclonic circulation over the northwestern Pacific during the boreal winter, which is reversed in La Niña years [*Cheung et al.,* 2012; *Li,* 1990; *Wen et al.,* 2000]. On the other hand, a stronger (weaker) EAWM promotes the occurrence and development of El Niño (La Niña) events [*Li et al.,* 2005; *Zhou et al.,* 2007].

On the interdecadal to decadal timescale, meteorological observations indicate a significant correlation between ENSO and EAWM [*He and Wang,* 2013; *Kim et al.,* 2016; *Wang et al.,* 2012a]. Much effort has been made to understand the long-term variability of the EASM using records from loess-paleosol sequences [eg. *Ding et al.,* 1995; *Sun et al.,* 2010; *Xiao et al.,* 1995], lacustrine sediments [eg. *Liu et al.,* 2009; *Wang et al.,* 2012b], stalagmites [*Sone et al.,* 2013] and marine sediments [eg. *Huang et al.,* 2011; *Steinke et al.,* 2011; *Yamamoto et al.,* 2013]. On longer time scales, however, only a few studies have examined possible links between ENSO and the EAWM based on climate model simulations and sediment records from low latitude regions [*An et al.,* 2017; *Xu et al.,* 2009; *Zheng et al.,* 2014]. In addition, there is a distinct lack of records from the most active region of the EAWM such as the mid-high latitudes of continental Asia.

© 2019 American Geophysical Union. All rights reserved.

The distribution of modern vegetation in Northeast China is significantly influenced by winter temperatures; for example, the boundary between the boreal forest and temperate deciduous forest, such as on the eastern margin of the Great Khingan Mountain Range, is largely determined by winter temperature [*Du et al.,* 2011]. Here we present a winter-temperature-sensitive pollen record from a Holocene lake sediment core from Lake Moon, Northeast China. We use the record to reconstruct the evolution of the EAWM in the Holocene, and to investigate the teleconnection between the EAWM and the ENSO on centennial/millennial timescales.

2 Materials and Methods

2.1 Study site

Lake Moon (47°30.36′N, 120°51.99′E, 1190 m above sea level) is in the Arxan-Chaihe volcanic field in the central part of the Great Khingan Mountain Range (Figure 1), 33 km from Chaihe Town, Zhalantun City, Inner Mongolia. The lake is a crater lake located in a scoria cone [*Sun et al.,* 2017], whose surface area is ~0.03 km^2, the maximum water depth is 6.5 m, and there is no inflow or outflow. The annual precipitation is ~300–600 mm and the mean annual temperature is -4–0 ºC with extremely low temperatures in January, from -32–-20 ºC. The vegetation surrounding Lake Moon is boreal deciduous broadleaf-conifer mixed forest, dominated by *Larix gmelinii* (Dahurian larch), *Betula platyphylla* (Siberian silver birch) and *B. dahurica* (Asian black birch), which can resist the long cold winter.

2.2 Sediment cores and chronology

An 886-cm sedimentary sequence, comprising three overlapping piston cores, was obtained from the center of Lake Moon in March 2007. The chronology of the core is based on 21 AMS ^{14}C dates from terrestrial and aquatic plant macrofossils and bulk sediment; the dating was conducting at Poznan Radiocarbon Laboratory [*Liu et al.,* 2010; *Wu and Liu,* 2012; *Wu et al.,* 2016] (see Supporting Information Table S1). The lithology of the upper 544 cm consists of dark-brown finely laminated gyttja in Holocene. In this study, a new age-depth model is established by Bacon V2.2 [*Blaauw and Christen,* 2011], a Bayesian approach based on all the radiocarbon ages previously published (see Supporting Information Figure S1).

2.3 Methods

2.3.1 Pollen analysis

Pollen analysis was conducted at a 2-cm interval. The samples were prepared using standing alkali and acid treatments [*Moore,* 1991]. Pollen grains were identified using an optical microscope at ×400 magnification with the aid of pollen atlases and keys [*Wang et al.*, 1995; *Wang and Wang,* 1983]. More than 400 terrestrial pollen grains were counted for most samples. Pollen percentages for each taxon were calculated using the sum of terrestrial pollen grains. In addition to the previously published pollen data [*Wu and Liu,* 2012], we got new data from the upper 50 cm of the sequence to obtain the pollen record from the Lake Moon spanning the Holocene.

2.3.2 Data analysis

Spearman rank correlation coefficients [*Press et al.,* 1992] were used to examine the relationship between variations in the frequencies of tree pollen taxa especially sensitive to the EAWM (*Pinus* and *Quercus*) and a time series of ENSO events. Non-parametric statistics were chosen because the data sets do not exhibit Gaussian distributions. As the calculation of

© 2019 American Geophysical Union. All rights reserved.

Spearman rank correlation coefficients could only be performed between records with the same resolution, the percentages of the *Pinus* and *Quercus* records and ENSO records resampled at a 20-year resolution based on interpolation. In addition, wavelet analysis [*Torrence and Compo,* 1998] of the *Pinus* and *Quercus* records was used to provide a simultaneous representation of the data in the time and frequency domains and thus to investigate the possible localization of cyclic patterns. Prior to the wavelet analysis, the *Pinus* and *Quercus* time series were resampled at a 10-year resolution based on interpolation and filtered to remove false cycles. The wavelet analysis was conducted using wavelet package in Matlab software.

3 Results and Discussion

3.1 Pollen records

272 pollen samples were analyzed, spanning the last 10.8 cal ka BP, with an average time resolution was 40 a. A simplified pollen diagram for Lake Moon is presented in Figure 2, whose data are available from Supporting Information Table S2. The pollen spectra can be grouped into the following vegetation categories: cold temperate boreal forest, temperate forest, mesic herbs, and xerophytic shrubs and herbs. Cold temperate boreal forest taxa mainly comprise *Betula* and *Alnus*, while the temperate forest taxa include *Pinus* and *Quercus*. Mesic herbs mainly comprise Poaceae, Cyperaceae and *Thalictrum*. Xerophytic shrubs and herbs comprise *Artemisia*, Chenopodioideae (Chenopodiaceae), *Ulmus* and *Ephedra*. The pollen record indicates that the vegetation in the central part of the Great Khingan Mountain Range was forest-steppe throughout the Holocene. Nonetheless there are significant changes in the proportions of the taxa representing the four groups of plant communities described above, the most prominent of which is the significantly higher frequencies of *Pinus* and *Quercus* since ca. 6.0 ka cal BP (Figure 2) compared to their extremely low representation in the early Holocene.

3.2 Proxies of the East Asian winter monsoon

Previous studies have shown that broad-leaved deciduous taxa, such as *Betula,* and boreal forest taxa, such as *Larix,* have a high degree of cold tolerance [*Prentice et al.,* 1992; *Sakai,* 1979; *Sakai and Weiser,* 1973]. In the present study area, the modern vegetation, i.e., deciduous broadleaf-conifer mixed forest dominated by *Larix gmelinii* and *Betula* spp., is habituated to the long and cold winter (For reference, from 1946–1999, there were 85 days altogether with a daily minimum air temperature of less than -40 ºC at the study site - www.hadobs.org). In contrast, temperate forest trees such as *Pinus* and *Quercus*, which are only sporadically present in the Great Khingan Mountain Range at the present day, are damaged by spontaneous ice nucleation below -40 ºC [*Sakai and Weiser,* 1973]; thus, the winter temperature is a crucial limiting factor for their survival in mid-high latitude regions. Therefore, the immigration of *Pinus* and *Quercus* into the cold temperate boreal forest represents an increase in the winter temperature, and is linked to the weakening of the EAWM. The extension of *Pinus* and *Quercus* is not only recorded at Lake Moon, but also in other lake sediment records from the mid-high latitude region of the Far East after 6.0 ka cal BP, for example at Tianchi Lake, Sihailongwan Maar Lake, Lake Kolotel (Figure 1 and Figure3c-f) and Jinchuan peat bog [*Jiang et al.,* 2008; *Stebich et al.,* 2015; *Tarasov et al.,* 2009; *Zhou et al.,* 2016]. The contents of *Pinus* and *Quercus* in pollen assemblages at these sites are also likely to be inversely correlated with the strength of the EAWM.

© 2019 American Geophysical Union. All rights reserved.

The trends in *Pinus* and *Quercus* at Lake Moon are synchronous with other EAWM indicators from low latitudes in the East Asian Monsoon (EAM) region, such as at Fukugaguchi Cave [*Sone et al.,* 2013] (Figure 3g) and Huguang Maar Lake [*Wang et al.,* 2012] (Figure 3h). This synchronous behavior clearly demonstrates a weakening of the EAWM at ~6.0 ka cal BP, confirming the reliability of the pollen proxies as an indicator of the EAWM, and indicating a teleconnection of climate change in mid-high latitudes and low latitudes of the EAM region.

3.3 Factors of the East Asian winter monsoon weakening since mid-Holocene

The increasing percentages of *Pinus* and *Quercus* at Lake Moon clearly demonstrate the weakening of the EAWM since ~6.0 ka cal BP. This trend is consistent with that of increasing winter (December-January-February) insolation at the latitude of study site throughout the entire Holocene [*Berger and Loutre,* 1991] (Figure 4a; black line), which provides a partial explanation for the warmer winter temperatures in Northeast China after ~6.0 ka cal BP.

Secondly, the sea surface temperature (SST) of the western tropical Pacific Ocean could also affect the intensity of the EAWM. The SST in the western tropical Pacific Ocean has dropped ~0.5 °C over the past 10.0 ka BP [*Stott et al.,* 2004] (Figure 4c; dark blue line). The cooling SST would reduce the land-sea thermal contrast between Pacific and Siberian air masses in winter, which weaken the strength of the EAWM under the assumption of constant Siberian high.

However, the relatively gradual changes in winter insolation and the SST of the western tropical Pacific Ocean cannot entirely explain the relatively abrupt weakening of the EAWM at 6-5 ka cal BP represented from this study, Huguang Maar Lake [*Wang et al.,* 2012] and Fukugaguchi Cave [*Sone et al.,* 2013]. Thus, other potential factors, like ENSO variability on centennial/millennial timescales need to be considered (Figure 4b; Cobb and Charles, 2013; Moy et al., 2002). The results of spearman rank correlation between 11 major pollen taxa from Lake Moon and two time series of ENSO events from the Laguna Pallcacocha, Ecuador [*Moy et al.,* 2002] and the Northern Line Islands [*Cobb and Charles,* 2013] were presented in Table 1. Higher correlation coefficients (0.616, 0.619, 0.426 and 0.418) imply highly significant relationships between percentages of *Pinus* and *Quercus* and frequencies of El Niño events, respectively. These results reveal a relatively strong relationship between the EAWM and ENSO events on centennial/millennial timescales.

3.4 ~500-year cycles of the East Asian winter monsoon

In this study, the results of wavelet analysis and band-pass filtering of the *Pinus* and *Quercus* records from Lake Moon are illustrated in Figure 5. The results show a period of low variance (blue and green color) from 10.8 to 6.0 ka cal BP, and a period of high variance (yellow and red color) after ~6.0 ka cal BP (Figure 5a, 5c and 5e). A prominent feature of the wavelet analysis is that a ~500-year quasi-periodic component exhibits stronger variance after ~6.0 ka cal BP (Figure 5a and 5c), and a 400-600 year-band-pass filter of the data reveals the same phenomenon (Figure 5b and 5d). These results indicate that ca. 500-year cycle exists in the intensity change of the EAWM. A similar periodicity has been noted previously in other Holocene palaeoclimate records from Northeast China, including plant cellulose in peat deposits [*Hong et al.,* 2001] and pollen records from maar lakes in Longgang Volcanic Field [*Xu et al.,* 2014; *Stebich et al.,* 2015]. This periodicity is evident in the proxy records of the EASM including summer temperature and rainfall; in this study it is also evident in a record of the EAWM.

© 2019 American Geophysical Union. All rights reserved.

The wavelet analysis and the band-pass filter of the frequencies of El Niño events recorded in the sedimentation from Laguna Pallcacocha, Ecuador (Figure 5e and 5f, *Moy et al.*, 2002) also present similar results with the proxies of the EAWM, that a ~500-year quasi-periodic component exhibits stronger variance after ~6.0 ka cal BP (Figure 5e and 5f). All these results indicate that the variance of ca. 500-year cycle becomes greater both in the intensity change of the EAWM and the frequencies of the ENSO events after ~6.0 ka cal BP.

Ca. 500-year cycle originates from changes in solar output [*Steinhilber et al.,* 2012; *Stuiver et al.,* 1995], which affects the dynamics of atmospheric and oceanic processes [*Chapman et al.,* 2000; *Cheng et al.,* 2016; *Wang et al.,* 2005; *Zhu et al.,* 2017]. The amplitude of variation of ~500-year quasi-periodic component of solar output before ~6 ka cal BP is greater than that after, which was not detected in the climate records in Northeast China in early Holocene in previous and this study [*Xu et al.,* 2014; *Stebich et al.,* 2015]. This phenomenon indicates that the EAM system is closely linked to the high-latitudes processes in early Holocene, mainly the global ice volumes, while the impacting of the tropical teleconnection between ENSO and the EAM system becomes more significant during the mid-late Holocene with the decreased global ice volumes [*Wang et al.,* 2012]. The anomalous anticyclone located in the western North Pacific has existed since ~6 ka cal BP as the bridge between ENSO and the EAWM, which is joint with strong southerly winds along the East Asian coasts weakened the EAWM significantly [*Wang et al.,* 2000; *Wang et al.,* 2012]. On these views, it is believe that the variation of solar output makes the weakening of the Walker circulation, the increasing of El Niño events and the shrinkage of the EAWM since the mid-Holocene. This transition is synchronous with the onset of the "modern" ENSO [*Sandweiss et al.,* 2001; *Moy et al.,* 2002] and also is widely acknowledged globally in the mid-Holocene [*Steig,* 1999; *Mayewski et al.,* 2004] as the termination of the Holocene thermal maximum, the hemispheric even global cooling, drier conditions in central to eastern Asia and Africa under the abrupt weakening of the monsoonal system, wetter conditions in northern Europe and southern South America [*Magny et al.,* 2006; *Roland et al.,* 2015, *Zhou et al.,* 2016]. The synchronicity of all these transitions implies that a reorganization in the Earth's ocean-atmosphere circulation system occurred in the mid-Holocene. This global event was ascribed to variations in solar activity, orbitally-driven insolation changes [*Hodell et al.,* 2001; *Magny and Haas,* 2004; *Mayewski et al.,* 2004; *Wanner et al.,* 2008] or non-linear feedback processes within the climate system components, especially changes in ocean circulation (e.g. NAO, ITCZ, ENSO) [*Schneider,* 2004; *Wunsch,* 2006; *Holmes et al.,* 2011]. Based on this study, the climate transition in the mid-Holocene is caused by the variations in solar activity and amplified by ocean circulation ENSO to influence the EAM system, and then change the vegetation in Great Khingan Mountain Range, Northeast China.

4 Conclusions

We have obtained a time series of warm winter events since 10.8 cal ka BP based on the changes in the frequencies of *Pinus* and *Quercus* pollen in the sediments of Lake Moon, in Northeast China. The data provide a robust record of changes in EAWM intensity in the mid-high latitude region of the EAM and it extends the timescale of a teleconnection between El Niño events and the EAWM from interannual/interdecadal to centennial/millennial.

The results of correlation analysis indicate that the EAWM weakened after 6.0 cal ka BP which was also related to the frequency of El Niño events on centennial/millennial timescales. Furthermore, the enhancement of El Niño events was the result of the increased prominence of the ~500-year cycle in solar output during the mid-Holocene.

© 2019 American Geophysical Union. All rights reserved.

Based on the results from this study, the climate transition in the mid-Holocene is caused by the variations in solar activity and amplified by ocean circulation ENSO to influence the intensity of the EAWM, and change the vegetation in Great Khingan Mountain Range, Northeast China.

Acknowledgments

This work was supported by the National Natural Science Foundation of China (41572353, 41320104006 and 41561144010) and Yunnan project for the introduction of advanced talents (2013HA024). We would like to thank Alan Sandford Palmer as well as another anonymous reviewer for their constructive comments and suggestions. The pollen data from Lake Moon in Holocene are available from Supporting Information Table S2.

References

An, S.-I., H.-J. Kim, W. Park, and B. Schneider (2017), Impact of ENSO on East Asian winter monsoon during interglacial periods: effect of orbital forcing, Clim. Dyn., 1-11, doi:10.1007/s00382-016-3506-8.

Berger, A., and M. F. Loutre (1991), Insolation values for the climate of the last 10 million years, Quat. Sci. Rev., 10(4), 297-317, doi:http://dx.doi.org/10.1016/0277-3791(91)90033-Q.

Blaauw, M., and J. A. Christen (2011), Flexible paleoclimate age-depth models using an autoregressive gamma process, Bayesian Analysis, 6(3), 457-474.

Chapman, M. R., Shackleton, and N. J. (2000), Evidence of 550-year and 1000-year cyclicities in North Atlantic circulation patterns during the Holocene, Holocene, 10(3), 287--291.

Cheng, H., A. Sinha, S. Verheyden, F. H. Nader, X. L. Li, P. Z. Zhang, J. J. Yin, L. Yi, Y. B. Peng, and Z. G. Rao (2016), The climate variability in northern Levant over the past 20,000 years, Geophys. Res. Lett., 42(20), 8641-8650.

Cheung, H. N., W. Zhou, H. Y. Mok, and M. C. Wu (2012), Relationship between Ural-Siberian Blocking and the East Asian Winter Monsoon in Relation to the Arctic Oscillation and the El Niño-Southern Oscillation, J. Clim., 25(12), 4242-4257.

Cobb, K. M., and C. D. Charles (2013), Highly variable El Niño-Southern Oscillation throughout the Holocene, Science, 339(6115), 67-70.

Ding, Z., T. Liu, N. W. Rutter, Z. Yu, Z. Guo, and R. Zhu (1995), Ice-Volume Forcing of East Asian Winter Monsoon Variations in the Past 800,000 Years, Quaternary Res., 44(2), 149-159, doi:http://dx.doi.org/10.1006/qres.1995.1059.

Du, H., Z. Wu, and M. Li (2011), Interdecadal changes of vegetation transition zones and their responses to climate in Northeast China, Theor. Appl. Climatol., 106(1), 179, doi:10.1007/s00704-011-0432-x.

He, S., and H. Wang (2013), Oscillating Relationship between the East Asian Winter Monsoon and ENSO, J. Clim., 26(24), 9819-9838.

Hodell, D. A., S. L. Kanfoush, A. Shemesh, X. Crosta, C. D. Charles, and T. P. Guilderson (2001), Abrupt Cooling of Antarctic Surface Waters and Sea Ice Expansion in the South Atlantic Sector of the Southern Ocean at 5000 cal yr B.P, Quaternary Res., 56(02), 191-198, doi:10.1006/qres.2001.2252.

© 2019 American Geophysical Union. All rights reserved.

Holmes, J., J. Lowe, E. Wolff, and M. Srokosz (2011), Rapid climate change: lessons from the recent geological past, Global. Planet. Change., 79(3), 157-162, doi:https://doi.org/10.1016/j.gloplacha.2010.10.005.

Hong, Y. T., Z. G. Wang, H. B. Jiang, Q. H. Lin, B. Hong, Y. X. Zhu, Y. Wang, L. S. Xu, X. T. Leng, and H. D. Li (2001), A 6000-year record of changes in drought and precipitation in northeastern China based on a δ13C time series from peat cellulose, Earth. Planet. Sc. Lett., 185(1), 111-119, doi:http://dx.doi.org/10.1016/S0012-821X(00)00367-8.

Huang, E., J. Tian, and S. Steinke (2011), Millennial-scale dynamics of the winter cold tongue in the southern South China Sea over the past 26 ka and the East Asian winter monsoon, Quaternary. Res., 75(1), 196-204, doi:http://doi.org/10.1016/j.yqres.2010.08.014.

Jiang, W., S. A. G. Leroy, N. Ogle, G. Chu, L. Wang, and J. Liu (2008), Natural and anthropogenic forest fires recorded in the Holocene pollen record from a Jinchuan peat bog, northeastern China, Palaeogeography, Palaeoclimatology, Palaeoecology, 261(1), 47-57, doi:https://doi.org/10.1016/j.palaeo.2008.01.007.

Kim, J.-W., S.-I. An, S.-Y. Jun, H.-J. Park, and S.-W. Yeh (2016), ENSO and East Asian winter monsoon relationship modulation associated with the anomalous northwest Pacific anticyclone, Clim. Dyn., doi:10.1007/s00382-016-3371-5.

Li, C. (1990), Interaction between Anomalous Winter Monsoon in East Asia and EI Nino Events, Adv. Atmos. Sci., 7(1), 36-46.

Li, C., S. Pei, and Y. Pu (2005), Dynamical impact of anomalous East-Asian winter monsoon on zonal wind over the equatorial western Pacific, Chinese Sci. Bull., 50(14), 1520-1526, doi:10.1360/04wd0327.

Liu, Q., Q. Li, L. Wang, and G. Q. Chu (2010), Stable carbon isotope record of bulk organic matter from a sediment core at Moon Lake in the middle part of Daxing'an Mountain range in Northeast China during the last 21 ka, Quaternary Sciences, 30(6), 1069-1077. (In Chinese with English abstract).

Liu, X., H. Dong, X. Yang, U. Herzschuh, E. Zhang, J.-B. W. Stuut, and Y. Wang (2009), Late Holocene forcing of the Asian winter and summer monsoon as evidenced by proxy records from the northern Qinghai–Tibetan Plateau, Earth. Planet. Sc. Lett., 280(1–4), 276-284, doi:http://doi.org/10.1016/j.epsl.2009.01.041.

Magny, M., and J. N. Haas (2004), A major widespread climatic change around 5300 cal. yr BP at the time of the Alpine Iceman, Journal of Quaternary Science, 19(5), 423-430, doi:10.1002/jqs.850.

Magny, M., U. Leuzinger, S. Bortenschlager, and J. N. Haas (2006), Tripartite climate reversal in Central Europe 5600–5300 years ago, Quaternary Res., 65(1), 3-19, doi:https://doi.org/10.1016/j.yqres.2005.06.009.

Mayewski, P. A., et al. (2004), Holocene climate variability, Quaternary Res., 62(3), 243-255, doi:https://doi.org/10.1016/j.yqres.2004.07.001.

Moore, P. D., J. A. Webb, and M. E. Collison (1991), Pollen analysis, 127-131 pp., Blackwell Scientific Publications.

© 2019 American Geophysical Union. All rights reserved.

Moy, C. M., G. O. Seltzer, D. T. Rodbell, and D. M. Anderson (2002), Variability of El Nino/Southern Oscillation activity at millennial timescales during the Holocene epoch, Nature, 420(6912), 162-165.

Prentice, I. C., W. Cramer, S. P. Harrison, R. Leemans, R. A. Monserud, and A. M. Solomon (1992), Special Paper: A Global Biome Model Based on Plant Physiology and Dominance, Soil Properties and Climate, J. Biogeogr., 19(2), 117-134.

Press, W. H., S. A. Teukolsky, B. P. Flannery, and W. T. Vetterling (1992), Numerical Recipes in FORTRAN: The Art of Scientific Computing, 95-96 pp., Cambridge University Press.

Roland, T. P., T. J. Daley, C. J. Caseldine, D. J. Charman, C. S. M. Turney, M. J. Amesbury, G. J. Thompson, and E. J. Woodley (2015), The 5.2 ka climate event: Evidence from stable isotope and multi-proxy palaeoecological peatland records in Ireland, Quat. Sci. Rev., 124(Supplement C), 209-223, doi:https://doi.org/10.1016/j.quascirev.2015.07.026.

Sakai, A. (1979), Freezing avoidance mechanism of primordial shoots of conifer buds, Plant. Cell. Physiol., 20(7), 1381-1390.

Sakai, A., and C. J. Weiser (1973), Freezing resistance of trees in North America with reference to tree regions, Ecology, 54(1), 118-126.

Sandweiss, D. H., K. A. Maasch, R. L. Burger, J. B. Richardson, Iii, H. B. Rollins, and A. Clement (2001), Variation in Holocene El Niño f equencies: Climate records and cultural consequences in ancient Peru, Geology, 29(7), 603-606, doi:10.1130/0091-7613(2001)029<0603:VIHENO>2.0.CO;2.

Schneider, S. H. (2004), Abrupt non-linear climate change, irreversibility and surprise, Global. Environ. Chang., 14(3), 245-258, doi:https://doi.org/10.1016/j.gloenvcha.2004.04.008.

Schulz, M., and M. Mudelsee (2002), REDFIT: estimating red-noise spectra directly from unevenly spaced paleoclimatic time series, Computers & Geosciences, 28(3), 421-426, doi:http://dx.doi.org/10.1016/S0098-3004(01)00044-9.

Schulz, M., and K. Stattegger (1997), Spectrum: spectral analysis of unevenly spaced paleoclimatic time series, Comput. Geosci.-UK, 23(9), 929-945, doi:http://dx.doi.org/10.1016/S0098-3004(97)00087-3.

Sone, T., A. Kano, T. Okumura, K. Kashiwagi, M. Hori, X. Jiang, and C.-C. Shen (2013), Holocene stalagmite oxygen isotopic record from the Japan Sea side of the Japanese Islands, as a new proxy of the East Asian winter monsoon, Quat. Sci. Rev., 75, 150-160, doi:http://doi.org/10.1016/j.quascirev.2013.06.019.

Stebich, M., K. Rehfeld, F. Schlütz, P. E. Tarasov, J. Liu, and J. Mingram (2015), Holocene vegetation and climate dynamics of NE China based on the pollen record from Sihailongwan Maar Lake, Quat. Sci. Rev., 124, 275-289, doi:https://doi.org/10.1016/j.quascirev.2015.07.021.

Steinhilber, F., J. A. Abreu, J. Beer, I. Brunner, M. Christl, H. Fischer, U. Heikkilä, P. W. Kubik, M. Mann, and K. G. Mccracken (2012), 9,400 years of cosmic radiation and solar activity from ice cores and tree rings, PNAS, 109(16), 5967.

Steinke, S., C. Glatz, M. Mohtadi, J. Groeneveld, Q. Li, and Z. Jian (2011), Past dynamics of the East Asian monsoon: No inverse behaviour between the summer and winter

© 2019 American Geophysical Union. All rights reserved.

monsoon during the Holocene, Global and Planetary Change, 78(3–4), 170-177, doi:http://doi.org/10.1016/j.gloplacha.2011.06.006.

Stott, L., K. Cannariato, R. Thunell, G. H. Haug, A. Koutavas, and S. Lund (2004), Decline of surface temperature and salinity in the western tropical Pacific Ocean in the Holocene epoch, Nature, 431(7004), 56-59, doi:http://www.nature.com/nature/journal/v431/n7004/suppinfo/nature02903_S1.html.

Stuiver, M., and T. F. Braziunas (1993), Sun, ocean, climate and atmospheric 14CO2 : an evaluation of causal and spectral relationships, The Holocene, 3(4), 289-305, doi:doi:10.1177/095968369300300401.

Stuiver, M., P. M. Grootes, and T. F. Braziunas (1995), The GISP2 δ18O Climate Record of the Past 16,500 Years and the Role of the Sun, Ocean, and Volcanoes, Quaternary Res., 44(3), 341-354, doi:http://dx.doi.org/10.1006/qres.1995.1079.

Stuiver, M., P. J. Reimer, E. Bard, J. W. Beck, G. S. Burr, K. A. Hughen, B. Kromer, G. McCormac, J. van der Plicht, and M. Spurk (1998), INTCAL98 radiocarbon age calibration, 24,000-0 cal BP, Radiocarbon, 40(3), 1041-1083.

Sun, C., Q. Liu, J. Wu, K. Németh, L. Wang, Y. Zhao, G. Chu, and J. Liu (2017), The first tephra evidence for a Late Glacial explosive volcanic eruption in the Arxan-Chaihe volcanic field (ACVF), northeast China, Quaternary Geochronology, 40, 109-119, doi:https://doi.org/10.1016/j.quageo.2016.10.003.

Sun, Y., X. Wang, Q. Liu, and S. C. Clemens (2010), Impacts of post-depositional processes on rapid monsoon signals recorded by the last glacial loess deposits of northern China, Earth. Planet. Sc. Lett., 289(1–2), 171-179, doi:http://doi.org/10.1016/j.epsl.2009.10.038.

Tarasov, P. E., E. V. Bezrukova, and S. K. Krivonogov (2009), Late Glacial and Holocene changes in vegetation cover and climate in southern Siberia derived from a 15 kyr long pollen record from Lake Kotokel, Clim. Past, 5(3), 285-295, doi:10.5194/cp-5-285-2009.

Timonen, M., J. Jiang, S. Helama, and K. Mielikäinen (2014), Significant changes of subseries-means in the Finnish tree-ring index of 7638 years, with comparisons to glaciological evidence from Greenland and Alps, Quaternary International, 319, 143-149, doi:http://dx.doi.org/10.1016/j.quaint.2013.02.006.

Wang, B., R. Wu, and X. Fu (2000), Pacific–East Asian Teleconnection: How Does ENSO Affect East Asian Climate? J. Clim., 13, 1517-1536.

Wang, H., and S. He (2012), Weakening relationship between East Asian winter monsoon and ENSO after mid-1970s, Chinese Science Bulletin, 57(27), 3535-3540.

Wang, F., N. Qian, and Y. Zhang (1995), Pollen morphology of plant in China, Science Press, Beijing. (In Chinese)

Wang, H., I. C. Prentice, and J. Ni (2013), Data-based modelling and environmental sensitivity of vegetation in China, Biogeosciences, 10(1), 5817-5830.

Wang, K., and X. Wang (1983), Palynology outline, Beijing, China: Peking University Press. Pp. (In Chinese).

Wang, L., et al. (2012), The East Asian winter monsoon over the last 15,000 years: its links to high-latitudes and tropical climate systems and complex correlation to the

© 2019 American Geophysical Union. All rights reserved.

summer monsoon, Quat. Sci. Rev., 32, 131-142, doi:http://doi.org/10.1016/j.quascirev.2011.11.003.

Wang, Y., H. Cheng, R. L. Edwards, Y. He, X. Kong, Z. An, J. Wu, M. J. Kelly, C. A. Dykoski, and X. Li (2005), The Holocene Asian Monsoon: Links to Solar Changes and North Atlantic Climate, Science, 308(5723), 854.

Wen, C., H.-F. Graf, and H. Ronghui (2000), The interannual variability of East Asian Winter Monsoon and its relation to the summer monsoon, Advances in Atmospheric Sciences, 17(1), 48-60, doi:10.1007/s00376-000-0042-5..

Wu, J., and Q. Liu (2012), Pollen-recorded vegetation and climate changes from Moon Lake since Late Glacial, Earth Science, 37(5), 947-954. (In Chinese with English abstract).

Wu, J., Q. Liu, L. Wang, G. Q. Chu, and J. Q. Liu (2016), Vegetation and Climate Change during the Last Deglaciation in the Great Khingan Mountain, Northeastern China, Plos One, 11(1).

Wunsch, C. (2006), Abrupt climate change: An alternative view, Quaternary Res., 65(02), 191-203, doi:10.1016/j.yqres.2005.10.006.

Xiao, J., S. C. Porter, Z. An, H. Kumai, and S. Yoshikawa (1995), Grain Size of Quartz as an Indicator of Winter Monsoon Strength on the Loess Plateau of Central China during the Last 130,000 Yr, Quaternary Res., 43(1), 22-29, doi:http://dx.doi.org/10.1006/qres.1995.1003.

Xu, D., H. Lu, G. Chu, N. Wu, C. Shen, C. Wang, and L. Mao (2014), 500-year climate cycles stacking of recent centennial warming documented in an East Asian pollen record, Scientific reports, 4(1), 3611.

Xu, F. J., A. C. Li, and S. M. Wan (2009), The geological significance of environmental sensitive grain-size populations in the mud wedge of the East China Sea during the mid-Holocene, Acta Oceanologica Sinica, 129(1-2), 229-230.

Yamamoto, M., H. Sai, M. T. Chen, and M. Zhao (2013), The East Asian winter monsoon variability in response to precession during the past 150 000 yr, Climate of the Past, 9(6), 2777-2788.

Zheng, X., A. Li, S. Wan, F. Jiang, S. J. Kao, and C. Johnson (2014), ITCZ and ENSO pacing on East Asian winter monsoon variation during the Holocene: Sedimentological evidence from the Okinawa Trough, Journal of Geophysical Research Oceans, 119(7), 4410-4429.

Zhou, W., X. Wang, T. J. Zhou, C. Li, and J. C. L. Chan (2007), Interdecadal variability of the relationship between the East Asian winter monsoon and ENSO, Meteorology and Atmospheric Physics, 98(3), 283-293, doi:10.1007/s00703-007-0263-6.

Zhou, X., et al. (2016), Time-transgressive onset of the Holocene Optimum in the East Asian monsoon region, Earth. Planet. Sc. Lett., 456, 39-46, doi:https://doi.org/10.1016/j.epsl.2016.09.052.

Zhu, Z., J. M. Feinberg, S. Xie, M. D. Bourne, C. Huang, C. Hu, and H. Cheng (2017), Holocene ENSO-related cyclic storms recorded by magnetic minerals in speleothems of central China, Proceedings of the National Academy of Sciences of the United States of America, 114(5), 852.

© 2019 American Geophysical Union. All rights reserved.

Table 1 Spearman rank correlation coefficients for two ENSO indices [Moy et al., 2002; Cobb and Charles, 2013] and the frequencies of major pollen taxa at Lake Moon (20-year resolution). Bold indicates significant at the 0.1% level.

Spearman rank correlation	El Niño event (Moy et al., 2002)	Sand % (Cobb and Charles, 2013)
Pinus (%)	**0.616**	**0.426**
Quercus (%)	**0.619**	**0.418**
Alnus (%)	**0.262**	**0.313**
Betula (%)	-0.001	**-0.229**
Ulmus (%)	**-0.439**	**-0.365**
Ephedra (%)	**-0.498**	**-0.285**
Artemisia (%)	**-0.223**	-0.076
Chenopodiaceae (%)	0.032	**0.329**
Poaceae (%)	**0.167**	**0.177**
Cyperaceae (%)	**0.143**	**0.507**
Thalictrum (%)	**-0.188**	-0.082

© 2019 American Geophysical Union. All rights reserved.

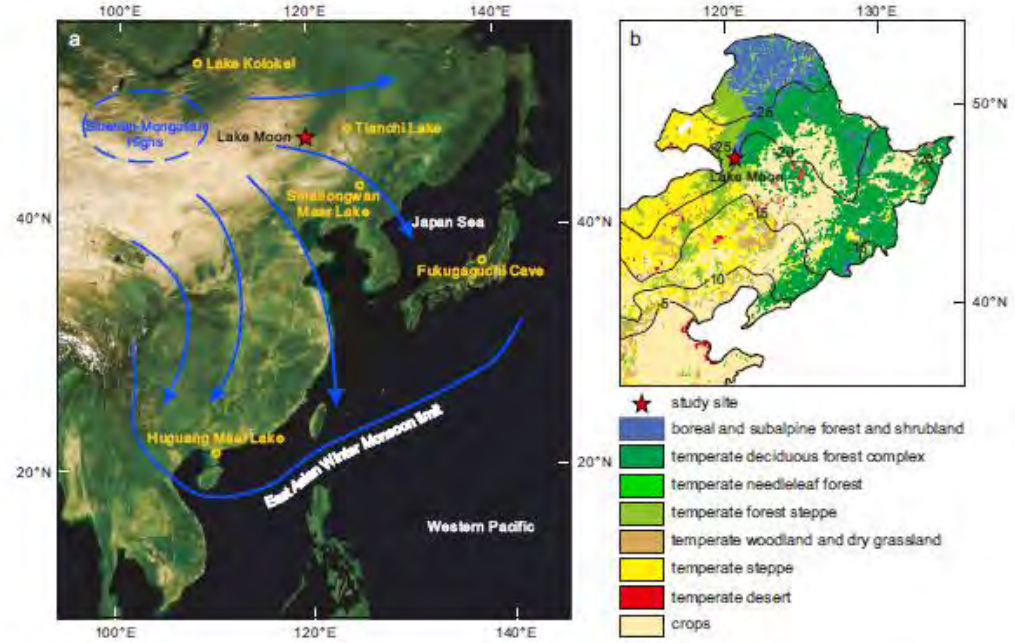

Figure 1. Location of Lake Moon. (**a**) Location of the study site and other palaeoclimatic records mentioned in the text. The trajectory of the EAWM is indicated by blue arrows; (**b**) Distribution of vegetation within the study region in northeast China [*Wang et al.*, 2013]; winter temperature contours are in degrees C.

© 2019 American Geophysical Union. All rights reserved.

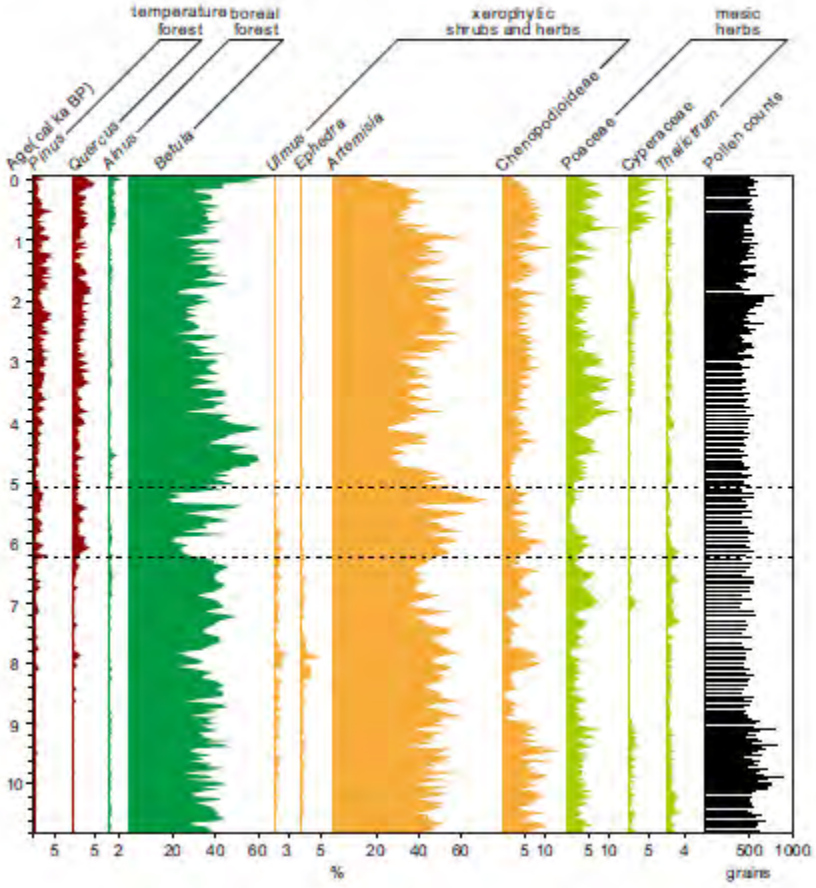

Figure 2. Simplified pollen percentage diagram for Lake Moon.

© 2019 American Geophysical Union. All rights reserved.

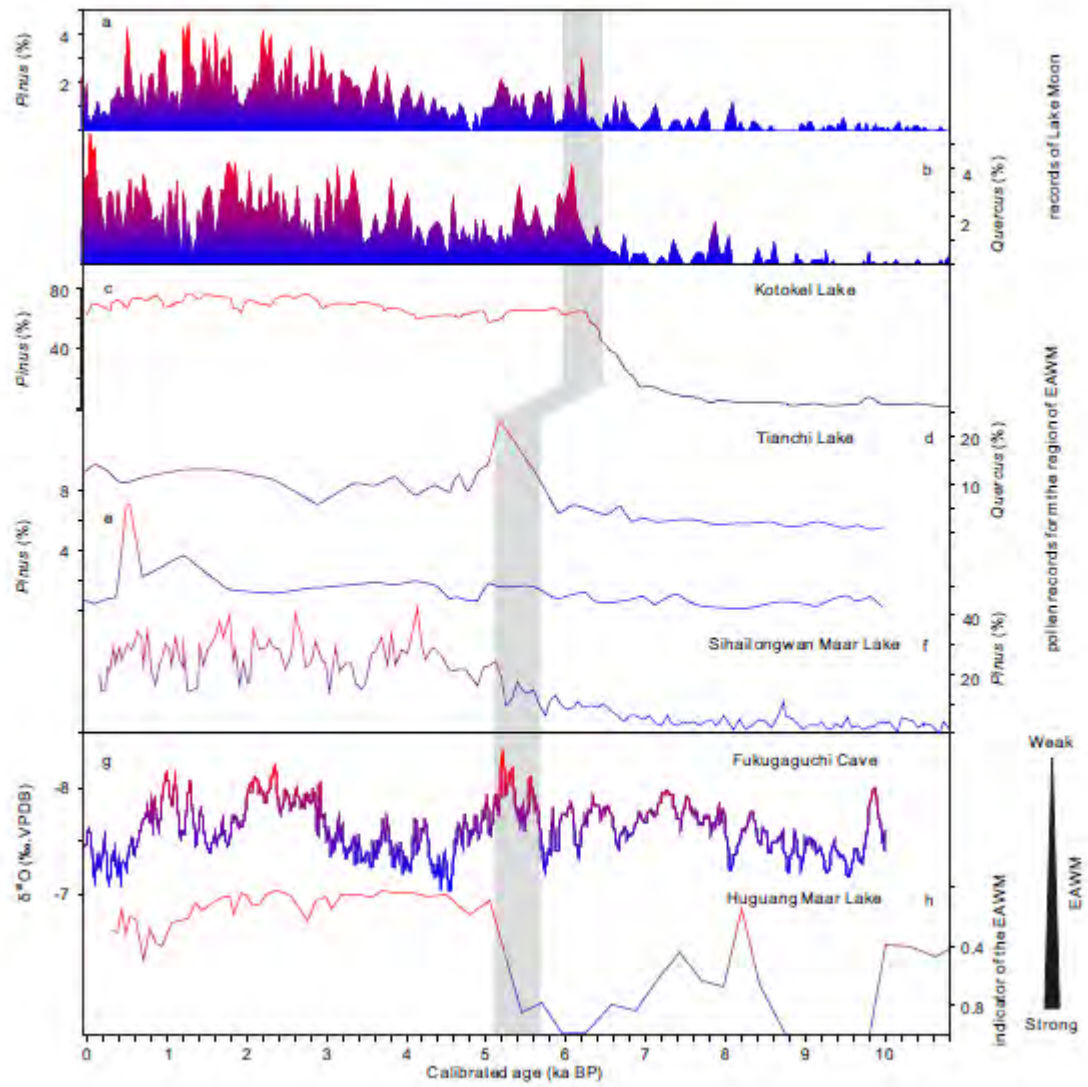

Figure 3. Time series of *Pinus* and *Quercus* frequencies at Lake Moon and other lake sites in mid-high latitudes of the EAM region compared with other EAWM proxies from the EAM region. (**a**, **b**) Records of *Pinus* and *Quercus* from Lake Moon (this study); (**c**) *Pinus* record from Lake Kotokel [*Tarasov et al.*, 2009]; (**d**, **e**) records of *Quercus* and *Pinus* from Tianchi Lake [*Zhou et al.*, 2016]; (**f**) *Pinus* record from Sihailongwan Maar Lake [*Stebich et al.*, 2015]; (**g**) $\delta^{18}O$ record (‰,VPDB) (5-point running average) from Fukugaguchi Cave [*Sone et al.*, 2013]; (**h**) EAWM indicator from Huguang Maar lake [*Wang et al.*, 2012b].

© 2019 American Geophysical Union. All rights reserved.

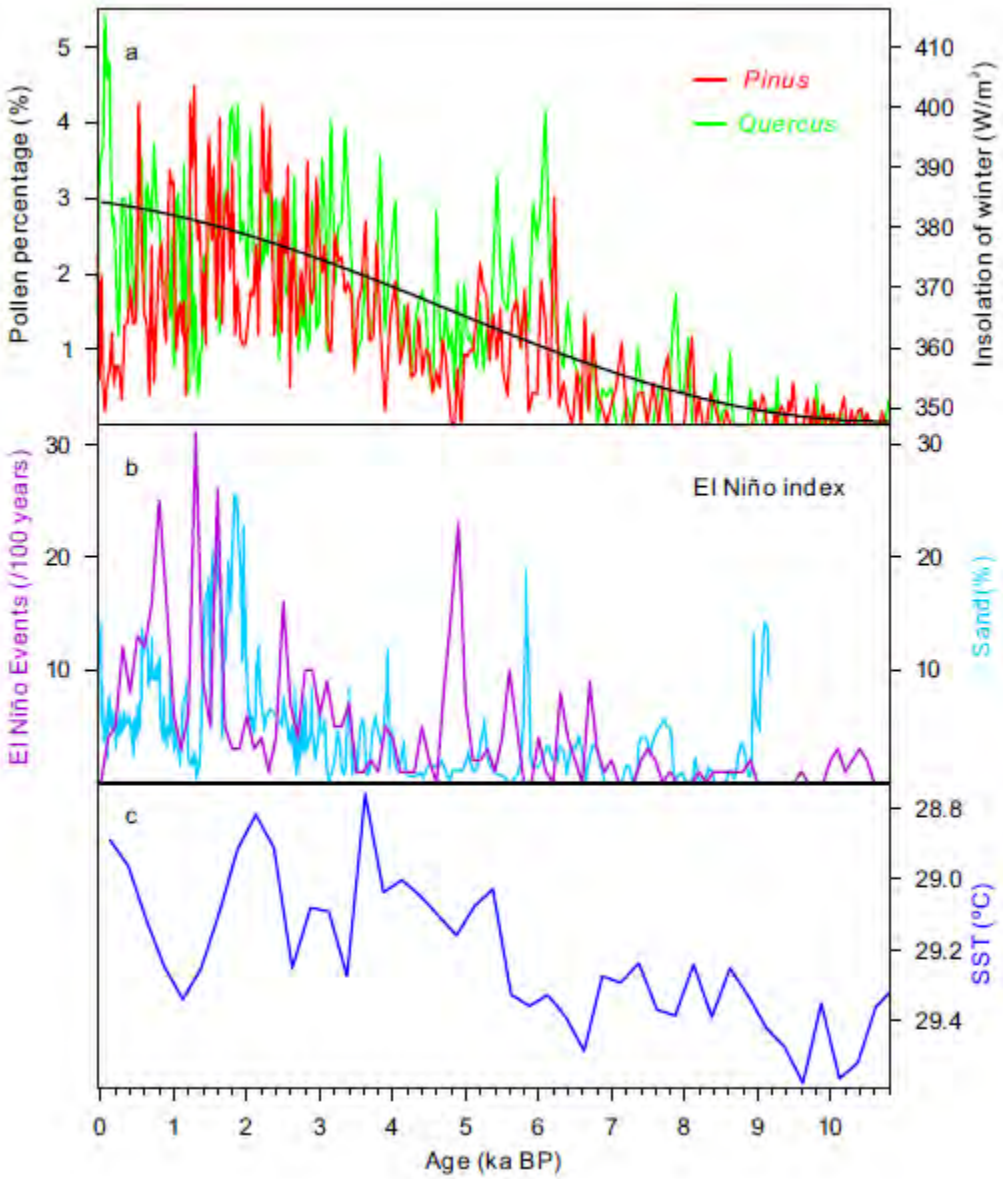

Figure 4. Comparison between the pollen records from Lake Moon with winter insolation at 45ºN, two ENSO indices and SST of the western tropical Pacific Ocean. (**a**) Pollen records of *Pinus* (red line) and *Quercus* (green line) from Lake Moon and winter insolation at 45ºN from *Berger and Loutre* [1991] (black line); (**b**) ENSO indices recorded by the lacustrine sediment from the Laguna Pallcacocha from *Moy et al.* [2002] (purple line) and the fossil coral records from the Northern Line Islands from *Cobb and Charles* [2013] (light blue line); (c) SST recorded by the oxygen isotope and Mg/Ca data from foraminifers in the western tropical Pacific Ocean from *Stott et al.* [2004] (dark blue line).

© 2019 American Geophysical Union. All rights reserved.

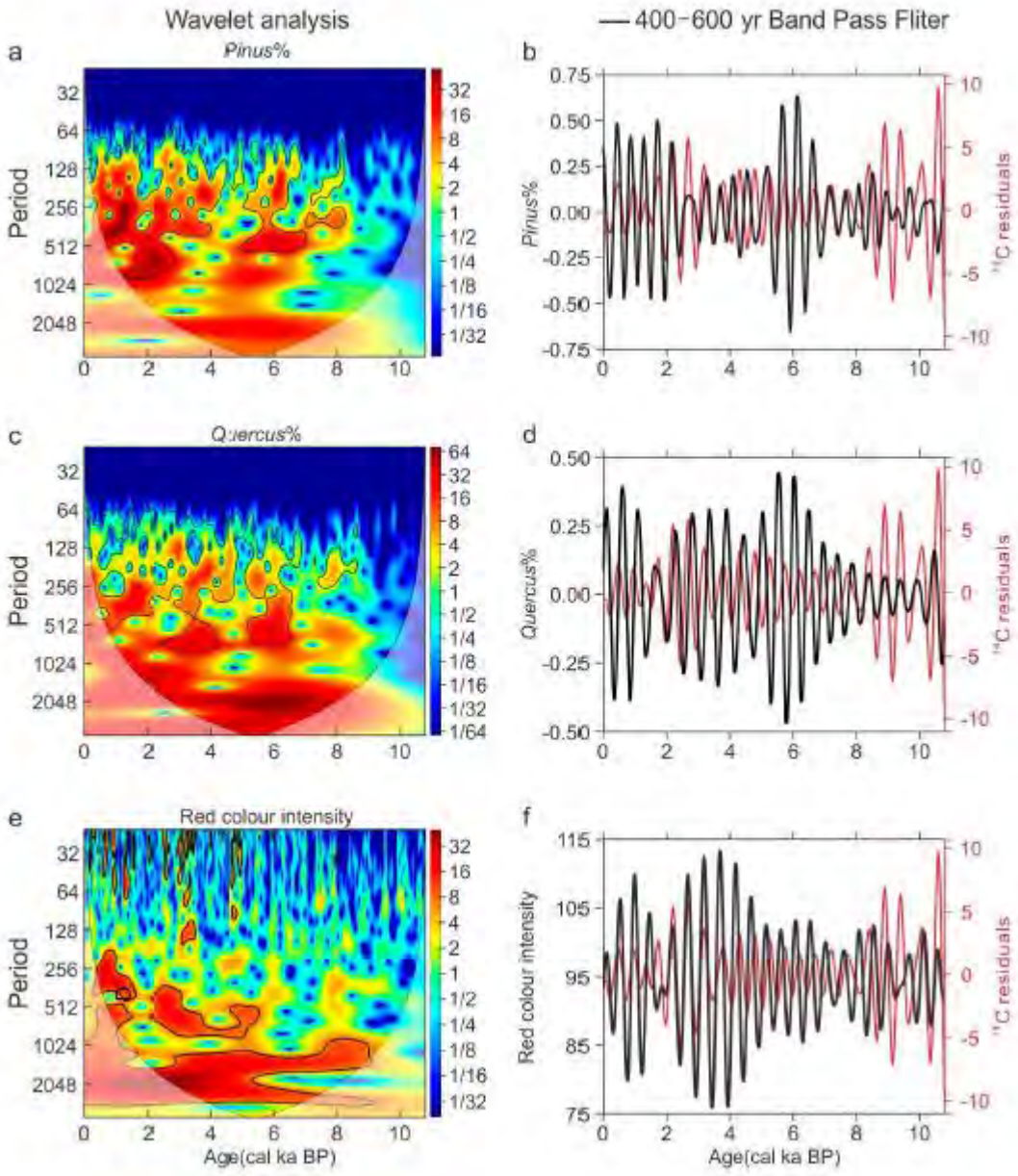

Figure 5. Wavelet spectrum and band-pass filtering calculated on pollen records and ENSO index. (**a-d**) Results of wavelet spectrum and band-pass filtering calculated on *Pinus* (%) and *Quercus* (%) record from Lake Moon; (**e**, **f**) Results of wavelet spectrum and band-pass filtering calculated on red color intensity record from the Laguna Pallcacocha from *Moy et al.* [2002]; the red line (**b**, **d**, **f**) is the results of the band-pass filtering calculated on the $\delta^{14}C$ residuals indicated the change of solar output [*Stuiver et al.*, 1998]. The wavelet power spectra for *Pinus* and *Quercus* were obtained after interpolation to evenly spaced data. The shape of the mother wavelet was set to Morlet. High (low) power is indicated by red (blue) color. High power can reach 32 or 64 values, while low power can be as low as 1/32 or 1/64 values. The 5% significance level against red noise is shown as a thick contour. The dark shaded area indicates the cone-of-influence, where edge effects become significant. This means the result of this area is unreliable.

© 2019 American Geophysical Union. All rights reserved.